Electrical characterization of Au/Ni Schottky contacts on GaN synthesized using electrodeposition

Abdulraoof I. Ali[1, 2*], Ezekiel Omotoso[1], Jacqueline M. Nel[1], Walter E. Meyer[1]

[1] *Physics Department, University of Pretoria, Pretoria 0002, South Africa*

[2]*Faculty of education, University of Elimam Elmahdi, Kosti White Nile, Sudan*

**Corresponding author e-mail address: abdalraof34@gmail.com,u18374710@tuks.co.za*

Abstract

Gallium nitride thin films have attracted attention due to their prospects in semiconductor devices and technology. In this study, we investigate the electrical properties and perform deep level transient spectroscopy (DLTS) on Au/Ni Schottky diodes fabricated on gallium nitride thin films that were synthesized by electrodeposition on a Si (111) substrate from a solution containing gallium nitrate ($Ga(NO_3)_3$) and ammonium nitrate ($NH_4(NO_3)$) using current densities of 1 and 3 mA/cm^2. The thin films were found to crystalize in the wurtzite hexagonal structure with crystallite sizes of approximately 20 nm. Scanning electron microscopy and atomic force microscopy were used to characterize the microstructure of the GaN thin films. The Schottky diodes had good rectifying properties, corresponding to n-type material. The diodes had a *IV* barrier heights of 0.76 eV and 0.60 eV; a *CV* barrier heights of 0.92 eV and 0.71 eV; and carrier densities of 1.2×10^{16} cm^{-3}, and 1.7×10^{16} cm^{-3}, for material deposited under 1 mA/cm^2 and 3 mA/cm^2, respectively. By fitting a model taking both thermionic emission as well as conduction through the polycrystalline bulk into account, it was found that the grain boundary potential of the GaN crystallites was 0.29 V.

The DLTS study revealed different dominant DLTS peaks in each as-grown sample with activation energies of 0.49 and 0.48 eV with capture cross-sections of 9×10^{-15} and 4×10^{-16} cm^2, in the material grown under 1 mA/cm^2 and 3 mA/cm^2 current density, respectively. The defects seem to be similar to defects found in heavily damaged GaN and GaN grown on highly mismatched or cracked substrates, and are probably not simple defects.

Keywords: Electrodeposition, GaN, DLTS, Defects, Schottky barrier diode.

1. Introduction

Group III-nitride semiconductor materials such as GaN, AlN and InN show potential in a variety of electronics applications, including diodes, transistors, LEDs, photovoltaic applications, optoelectronic devices, high power and high-temperature electronic devices [1], [2]. GaN is characterized by the high thermal stability of the wurtzite structure. The new generation of semiconductors relies heavily on nanotechnology and advances in nanomaterials.

Among the Group III-nitride materials, GaN is an important semiconductor material with a direct wide band gap. Many deposition techniques may be used to produce GaN, these include metalorganic chemical vapor deposition [3, 4], molecular beam epitaxy [5], hydride vapor phase epitaxy [6], radio-frequency magnetron sputtering [7] and atomic layer deposition [8]. However, these techniques are expensive, and require specialized processing systems. GaN thin films can also be synthesized by other techniques such as sol-gel [9] and electrodeposition [10, 11, and 12]. The advantages of electrodeposition include cost-effectiveness, minimum waste generation, long bath lifetime, easy set-up and that the thickness and surface morphology may be controlled by varying the deposition parameters. In addition, there currently is growing interest in wet chemical growth of semiconductors for use in applications such as printable electronics. Flexible electronics, which includes printable electronics, is seen as essential for the development of the Internet of Things [13]. Other applications of printable electronics include flat panel displays [14]. In general, printable electronics requires that semiconductors be grown by wet chemical techniques, therefore it is worthwhile investing various wet chemical growth techniques for semiconductors to be used in electrical applications. Metal-semiconductor junctions are arguably the simplest structures in electronic devices and form an essential component of most devices. Furthermore, Schottky diodes allow the material beneath the Schottky contact to be electrically characterized using DLTS. Therefore, in this study, we investigate the electronic properties of Schottky diodes on electrodeposited GaN.

GaN Schottky diode performance is influenced by the Schottky and ohmic contacts. The majority of work in this area is being done to improve their characteristic in order to obtain better device performance using different metals as Schottky contacts. A previous study used Au for Schottky contact on GaN thin films [15] and the Schottky diode was found to have an ideality factor, n, for the as-grown sample of 2.4 and a Schottky barrier height from the current-voltage (IV) and capacitance-voltage (CV) measurements, ϕ_B, of 0.58 eV and 1.18 eV respectively. In this study, we investigated room-temperature (300 K) electrodeposition growth of GaN using different current densities. In current paper we investigate the effect of using Au/Ni metal layers as the Schottky contact on the GaN thin films that were deposited using different current densities. The effect of Au/Ni on the electrical properties were studied by IV and CV measurements as well as DLTS and compared to other previous work.

Deep-level transient spectroscopy (DLTS) studies on GaN have been performed previously on materials grown by the more traditional methods mentioned previously [16, 17, 18, and 19],

but more still needs to be explored on the characterisation of deep level defects induced in electrodeposited GaN thin films using DLTS.

2. Experimental procedure

The GaN thin films were deposited on n-Si (111) substrates using electrodeposition. The Si substrate had an epitaxial layer 13 - 17 μm thick with a resistivity of 1.4 – 1.8 ohm.cm and a carrier concentration of 3.5×10^{15} cm^{-3} which was grown on an n^+ wafer, 0.5 mm thick. The GaN was grown on top of the epitaxial layer which was cleaned by washing sequentially in trichloroethylene, isopropanol, methanol, and deionized water for 5 minutes each and in HF (40 %) for 30 s. The deposition solution was 0.034 M gallium nitrate ($Ga(NO_3)_3$) and 0.025 M ammonium nitrate ($NH_4(NO_3)$) in deionized water at room temperature (300 K). The solution was thoroughly stirred to ensure a homogeneous solution. An activated carbon anode and the Si (111) substrate cathode were separated by 1 cm. A current density of either 1 or 3 mA/cm^2 was used during the deposition for 30 minutes. The resulting GaN films' structure and microstructure were characterized by X-ray diffraction (XRD) with Cu $K_{\alpha 1}$ radiation (λ = 1.54056 Å), and scanning electron microscopy using a Zeiss Ultra Plus (FEG, SEM), atomic force microscopy using a Bruker Dimension Icon (AFM) was used to characterize the morphology of deposited samples.

An Al ohmic contact of 140 nm thick and Ni/Au Schottky contacts (60/80 nm thick) were deposited using resistive evaporation on the GaN thin films. The Al was deposited while half the sample was masked off leaving space for the Schottky contacts, which were deposited through a metal contact mask with holes 0.6 mm in diameter. No annealing was done. The electrical characterization was performed using *IV* and *CV* measurements in the dark, using an HP4140B pA meter/DC voltage source and an HP4192A LF Impedance Analyzer. The *CV* characteristics were measured using frequency of 1 MHz. The diode in Fig. 1 was also placed in a closed cycle helium cryostat to characterize the defects in the GaN using DLTS.

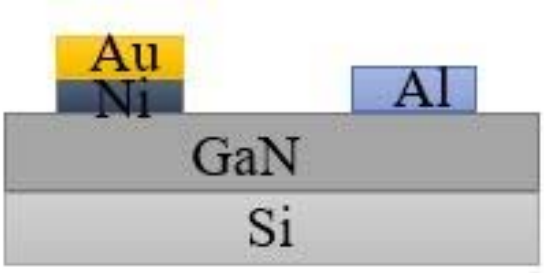

Figure: 1 A schematic diagram of the Schottky diode.

3. Results and discussion

Gallium nitrate and ammonium nitrate dissolve in water and are transported in the electrolyte when the electric field is applied as illustrated in the following reactions [11]

$$Ga(NO_3)_3 \longrightarrow Ga^{3+}(aq) + 3(NO_3)^-(aq)$$
$$NH_4NO_3 \longrightarrow NH_4^+(aq) + (NO_3)^-(aq)$$
$$NH_4^+ + (NO_3)^- \longrightarrow NH_3 + HNO_3$$
$$Ga(NO_3)_3 + NH_3 \longrightarrow GaN + 3HNO_3$$

As a result, relatively high concentrations of Ga^{3+} and NH_4^+ are present at the cathode (Si). GaN is formed on the surface of the cathode as these two ions come together. Clusters of critical sizes form, allowing continuous films to grow [11].

3.1 Structure and morphology of GaN thin films

The XRD of the GaN thin films grown at current densities of 1 and 3 mA/cm^2 for 30 minutes (identified as Samples *a* and Sample *b*, respectively) are shown in Fig. 2. The XRD patterns from JCPDS 50-0792 for h-GaN show good agreement with the GaN thin films prepared by electrodeposition. The prominent peaks in the spectrum of Sample *a* found at 33.96°, 37.30°, and 46.64° as well as the two small peaks at 31.73°, and 59.14°, correspond to the hexagonal wurtzite phase. One peak corresponding to c-GaN at 41.3° was also identified as seen in JCPDS 01-075-8381 while 45.56° could be corresponding to pure gallium [12]. The Si (111) peak was observed at 27.1°. The same peaks were observed in Sample *b* with a small shift to higher angles compared to Sample *a*. The GaN films in this study showed a mix of the hexagonal and the cubic phases which is in agreement with previous studies [10, 11, and 12]. The crystallite size of thin films increased from 19 to 22 nm as the current density increased from 1 mA/cm^2 to 3 mA/cm^2. In Fig. 2, it can be seen that there is shift in peaks position for Sample *a* (1 mA/cm^2) and Sample *b* (3mA/cm^2) this has been associated with the presence of both uniform and non-uniform strain. Higher current densities create more reductive conditions, which in turn increase the activation energy needed for deposition. This is more advantageous for the deposition of species controlled by kinetics than diffusion [20].

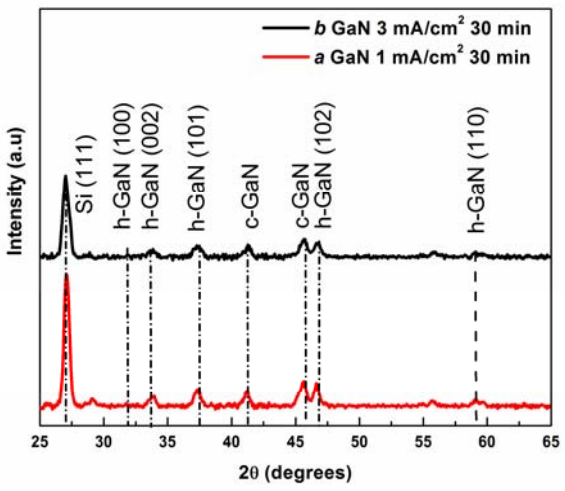

Figure 2: XRD spectra for the GaN thin films, Samples *a*, and *b* deposited at 1 mA/cm^2 and 3 mA/cm^2, respectively, for 30 minutes. Dashed lines correspond to h-GaN JCPDS 50-0792.

The structure parameters of the GaN thin films were obtained from XRD data in Fig. 2. The crystallite size was calculated using Sherrer's formula [21],

$$t = \frac{0.9\lambda}{B\cos\theta_B}, \tag{1}$$

where λ is the wavelength of the incident X-rays (1.54056 Å for Cu $K_{\alpha 1}$), θ_B is the Bragg angle and B is the full width at half maximum of the peak — in this case the (002) peak. The lattice constants were calculated using the formulas below and the results are shown in Table 1:

$$a = \frac{\lambda}{\sqrt{3}\sin\theta_B} \tag{2}$$

and

$$c = \frac{\lambda}{\sin\theta_B}. \tag{3}$$

The lattice constants, *a* and *c*, of the GaN thin film were compared to JCPDS 50-0792 and results obtained previously by Al-Heuseen *et al.* [11] in Table 1. The lattice constants in the present study decreased with increasing current density and moved closer to the reference values. A change in lattice constant could be due to strain [20]. As will be seen later, the SEM image for Sample *b* showed cracks that relax the strain, resulting in an XRD spectrum closer to the ideal.

Table 1: Structural parameters obtained from XRD patterns of the electrochemically deposited GaN thin films on Si substrate. Sample *a*, and Sample *b* deposited for 30 minutes at 1 and 3 mA/cm^2, respectively.

Sample	FWHM (°)	Peak Position, 2θ (°)	Peak origin	Average crystallite size, *t* (nm)	Lattice constants (Å)	
					a (100)	*c* (002)
JCPDS 50-0792	---	34.603	(002)	---	3.186	5.178
		36.962	(101)			
		48.20	(102)			
(Al-Heuseen *et al.*, 2010)	-	-	-	18 - 19	3.35	5.159
a	0.3926	33.968	(002)	19	3.25	5.27
	0.3365	37.257	(101)			
	0.2804	46.636	(102)			
b	0.2244	34.029	(002)	22	3.20	5.26
	0.8974	37.580	(101)			
	0.4487	46.866	(102)			

Fig. 3 shows the different surface morphologies of the GaN thin films on Si (111) substrates observed by scanning electron microscopy (SEM). Fig. 3a shows the surface of Sample *a* grown at 1 mA/cm^2 that had smaller fine grains that agglomerated together, while Fig. 3b shows the surface of Sample *b* grown at 3 mA/cm^2 that was smoother with cracks visible on the surface. This is in agreement with the two previous studies in which different current densities were used [11, 12], where lower current densities produced smaller grains, while higher current densities produced larger grains with cracks. In contrast with [12], who did not find any growth at a current density of 2.5 mA/cm^2, we found growth at a current density of 1 mA/cm^2, which agrees with the results of [10, 11], who found growth at current density of 1.5 mA/cm^2. The thickness of the thin film from the SEM cross section were found to be 350 nm to 400 nm.

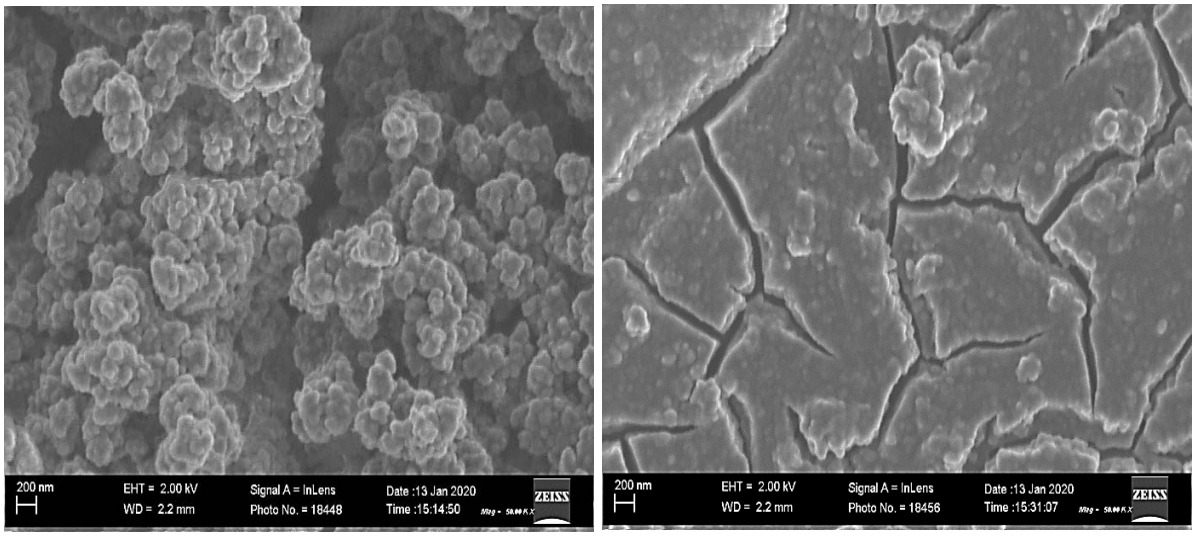

(a) (b)

Figure 3: Scanning electron micrograph images of GaN deposited under different conditions on a Si substrate for 30 minutes: (a) Sample *a* deposited at 1mA/cm^2 and (b) Sample *b* deposited at 3 mA/cm^2.

In Fig. 4, it can be seen that the morphologies of representative areas of the GaN thin films observed by AFM are different and that deposition conditions affect the morphology of thin films. The surface morphology of the GaN thin film in Sample *a* deposited using 1 mA/cm^2 (Fig. 4a) was not as smooth as that of Sample *b*, deposited using 3 mA/cm^2 (Fig. 4b) while Sample *b* had smaller grains (particles).

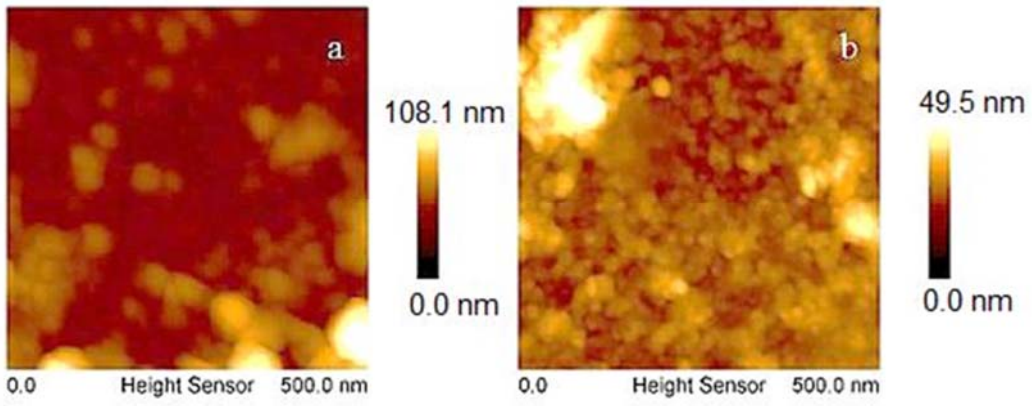

Figure 4: AFM images of GaN thin films deposited for 30 minutes: (a) Sample *a* deposited at 1 mA/cm^2 and (b) Sample *b* deposited at 3 mA/cm^2.

3.2 Electrical characterization

The properties of the Au/Ni/GaN Schottky diodes on the as-grown films were studied using current-voltage (*IV*) and capacitance-voltage (*CV*) measurements at room temperature. For ideal Schottky diodes, without series resistance, the thermionic emission model predicts a current [22]:

$$I = I_s \left[\exp\left(\frac{qV_d}{nkT}\right) - 1\right], \quad (4)$$

where I_s is the saturation current, T is the temperature, q is the electron charge, k is Boltzmann's constant, n is the ideality factor (which, in the ideal case, is close to unity) and V_d is the voltage across the diode.

From the *IV* plot in Fig. 5a, the Au/Ni/GaN/Al diodes deposited on both films were rectifying and the GaN was n-type. Table 2 gives a summary of the electrical properties of the Schottky diodes. The electrical properties of the samples *a* and b as shown in Fig. 5(a), were similar in terms of general shape. Under forward bias, for low biases, there was a linear region indicating thermionic emission which flattened at higher biases due to significant series resistance, while in the reverse direction relatively high leakage current was observed in Sample *b*. Sample *a*, deposited at 1 mA/cm^2 showed much better rectifying properties than Sample *b*, but also higher series resistance. Since the Si substrate had good conductivity, it is assumed that the series resistance measured was due to conduction perpendicularly through the GaN layer. Since reverse leakage current is often due to defects [23], the difference might be due to the material in Sample *a* having better quality due to the slower growth rate. The cracks in Sample *b* may also give rise to regions of lower barrier height, which would increase the reverse leakage current. Also, the more uneven structure of Sample *a* might explain its higher series resistance (416 Ω) compared to Sample *b* (241 Ω). The ideality factors of Au/Ni/GaN/Al as grown (Samples *a* and *b*) were 1.80 and 2.30, and were less than that obtained for the Au/GaN/Al Schottky diodes in previous study [15]. The Schottky barrier height were found to be 0.76 eV and 0.60 eV, respectively and were larger compared to those found in a previous study [15], however these were for pure gold contacts. The summary of the electrical properties of the Au/Ni/GaN/Al Schottky diodes compared to previous study [15] can be seen in Table 2. In Table 3 a comparison of the barrier heights of Schottky diodes on material grown by different growth techniques, are given.

As mentioned earlier, when the resistance of the semiconductor is not the restricting factor, the majority-carrier transport is governed by thermionic emission expression, Equation (4)

However, as current flow increases, restriction of current flow in the semiconductor becomes more important. The current through the semiconductor with multiple grain boundaries is described by Korsh & Muller [24]:

$$I = 2\,A\,A^{*}\,T^{2} \exp\left(-\frac{q\Phi_g}{kT}\right) \sinh\left(\frac{qV_b}{2NkT}\right), \quad (5)$$

where A is the area of the diode, A^* is the Richardson constant identified with thermionic emission across the grain boundaries, N is the number of grain boundaries involved, Φ_g is the grain boundary potential barrier, and V_b is the voltage across the bulk of the semiconductor.

In order to investigate the applicability of this model, we considered the above two processes to occur in series, i.e. that the current is the same for both processes, and the applied voltage V_a is the sum of the voltages due to the two processes,

$$V_a = V_d + V_b\,. \quad (6)$$

In fitting this model, it turns out that in Equation (5), N and Φ_g are strongly correlated and can't be used as independent parameters. We therefore decided to estimate N by assuming a layer thickness of 400 nm and crystallite size of 20 nm, leading to a layer thickness of approximately 20 crystallites. Since the current passes through the layer twice, we used $N = 40$.

Fig. 6a shows the result of fitting this model, while Fig 6b zooms in on a selected section. The parameters are summarised in Table 4. When fitted to the complete forward voltage range (solid line in Fig 6), it is clear that in the region in which the thermionic emission is the significant factor (i.e. for applied voltages less than 0.5 V), the fit is not good. This is especially the case for Sample *a*. This is also reflected in the parameters obtained for the thermionic emission part of the model, which agree well with those extracted earlier for Sample *b*, but differ significantly to those obtained for Sample *a*.

In an attempt to improve the fit, we restricted the fit to forward biases from 0.75 V, where we expect bulk effects to dominate. This only marginally improved the fit (see zoomed in section shown in Fig. 6b) and did not influence the value obtained for Φ_g significantly, although it did influence the parameters of the thermionic emission model significantly (see Table 4). In addition, the value of Φ_g did not differ significantly between Sample *a* and *b* and can be estimated at 0.29 V. Furthermore, the value of Φ_g only changed by a small amount when different values of N were used, e.g. changing N to 100 changed the value of Φ_g to 0.28 V.

We therefore conclude that the bulk conduction can be described by Equation (5), with grain boundary potential of 0.29 V, while it is also clear that the forward conduction of the Schottky diode is not explained well by simple thermionic emission. We speculate that this could be due to variations in the barrier height across the surface of the diode.

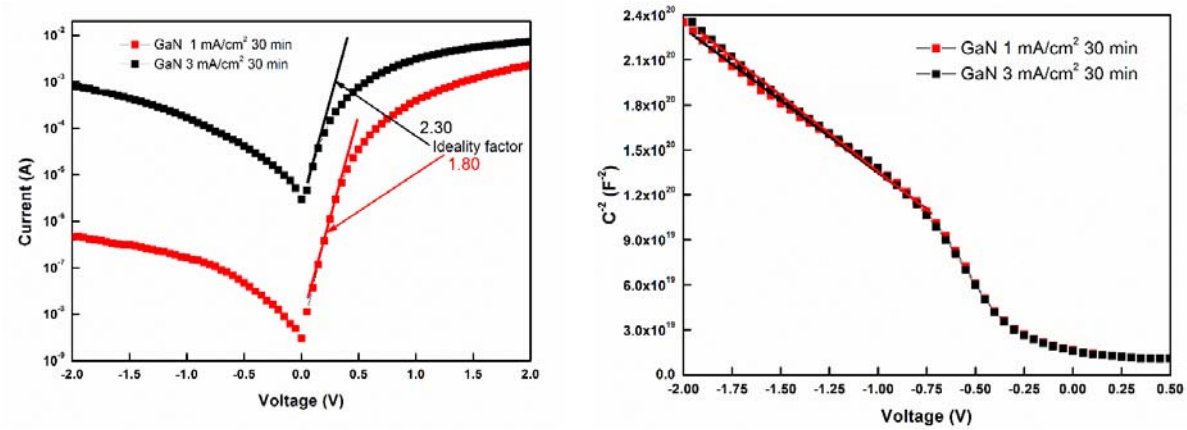

(a) (b)

Figure 5: (a) The semi-logarithmic forward and reverse bias *IV* plots (b) the plot of $1/C^2$ versus applied voltage of the Au/Ni/GaN Schottky barrier diodes at room temperature (300 K) for the as-grown films deposited at 1 mA/cm^2 and 3 mA/cm^2, respectively.

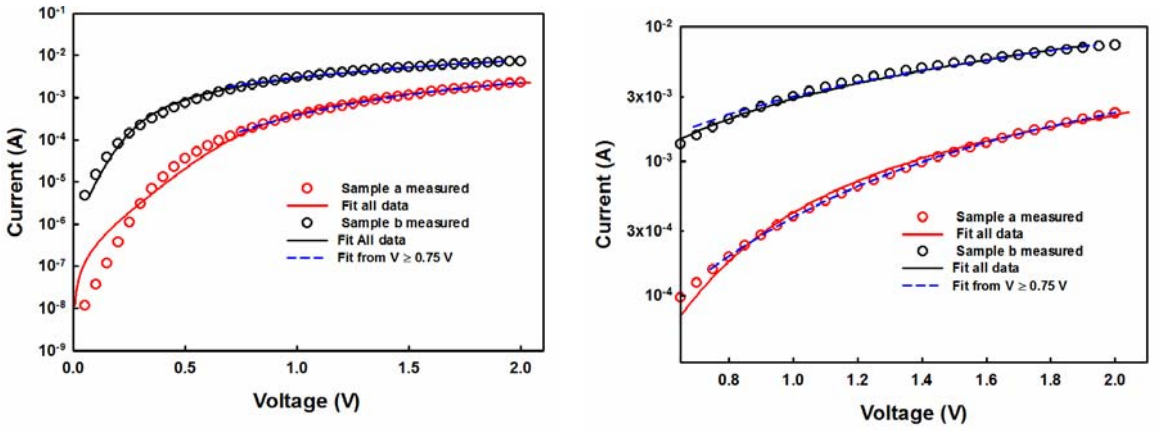

(a) (b)

Figure 6: The fitting of forward *IV* characteristics of both samples in the voltage range of 0 to 2 V (solid line) and 0.75 to 2 V (dashed line). Graph (a) shows the full range of the data, while Graph (b) zooms in on the 0.75 to 2 V range.

The Schottky barrier heights were also determined from the *CV* data (Fig. 5b). From the fitting of the $C^{-2}V$ plot in Fig. 5b, we obtained the Schottky barrier height to be 0.92 eV and 0.71 eV and carrier concentration was estimated to be 1.2×10^{16} cm^{-3} and 1.7×10^{16} cm^{-3}, for Samples *a* and *b*, respectively. Again, the lower carrier density might be related to Sample *a* having fewer defects.

We can conclude that the Au/Ni Schottky diodes perform better than the previous studied Au Schottky diodes [15], which we ascribe to better interface quality due to the better adhesion by Ni. It can be seen from our findings that the barrier height of the GaN Schottky diodes prepared by electrodeposition yielded comparable results to other researchers. This indicates that electrodeposition produces GaN thin films that can be used in the fabrication of devices. The Schottky barrier height from both the *IV* and *CV* measurements show a decrease with the increase in the current density during deposition.

Table 2: Summary of the electrical properties of Au/Ni/GaN/Al Schottky barrier diodes fabricated on the deposited films.

Sample	n	I_s (A)	ϕ (eV)		N_d (cm^{-3})	R_s (Ω)	Ref
			IV	*CV*			
d	2.40	1.20×10^{-6}	0.58	1.18	1.1×10^{18}	550	Previous work [15]
a	1.80	5.09×10^{-9}	0.76	0.92	1.2×10^{16}	416	Current study
b	2.30	2.43×10^{-6}	0.60	0.71	1.7×10^{16}	241	Current study

Table 3: A comparison with the reported literature on the fabrication of Schottky barrier diodes for GaN synthesized with different techniques.

Material	Growth technique	Ideality factor	Barrier height from *IV* (eV)	Schottky metal	Ref
GaN thin film	MOCVD	1.4	0.7	Ni	[25]
GaN thin film	MOCVD	2.9	0.45	Ni/Au	[26]
Ge:GaN thin film	RF reactive sputtering	4.05	0.6	Pt	[27]
GaN nanowires	CVD	12	0.48	Au	[28]
GaN nanowires	CVD	1.65	0.8	Ni/Au	[29]
GaN on GaN overlayer on sapphire	MBE	1.08-1.10	1.08-1.03	Ni	[30]
GaN thin film	ECD	2.40	0.58	Au	[15]
GaN thin film	ECD	1.80-2.30	0.76 - 0.60	Ni/Au	Current work

Table 4: The Parameters extracted from the fitting of the model by Korsh & Muller [24] to the forward *IV* characteristics of Samples *a* and *b*.

Sample	Fit region	Current saturation I_s (A)	Grain boundary potential ϕ_g (V)	Ideality factor n
Sample *a*	All	1.9×10^{-7}	0.30	4.0
	$V \geq 0.75$ V	6.2×10^{-6}	0.29	8.2
Sample *b*	All	1.3×10^{-6}	0.28	1.8
	$V \geq 0.75$ V	1.4×10^{-7}	0.29	1.0

3.3 DLTS results

The DLTS spectrum and Arrhenius plot of the defects found in GaN thin films grown by electrodeposition are shown in Figs 7a and 7b, respectively. The DLTS signal measured between 30 and 350 K is shown for Samples *a* and *b* at emission rate windows of 20 to 200 s^{-1} with a reverse bias of -2 V and pulse bias of 0 V. In the as-grown films, different prominent peaks were found in each of the thin films which were labelled E_a and E_b for Samples *a* and *b*, respectively.

The activation energy and capture cross-section of the defects were calculated using the emission rate equation [31, 32]:

$$\ln\frac{e_n}{T^2} = \ln\left(4\sqrt{6}\,\pi\,1.5\,k^2 m^* \sigma_n/h^3\right) + \left(\frac{\Delta E_n}{1000k}\right)1000/T \qquad (7)$$

where e_n is the emission rate, *T* is the absolute temperature, *k* is the Boltzmann constant, *m** is the effective mass of conduction electrons in GaN, *h* is Plank's constant, σ_n is the capture cross section and ΔE_n is the activation energy.

Fig. 7b shows the Arrhenius plots for defects in the as-grown GaN samples with activation energies of 0.49 eV and 0.48 eV, and capture cross sections of 8.6×10^{-15} and 4.5×10^{-16} cm^2, for E_a and E_b, respectively. Also shown are Arrhenius plots of some similar defects described in literature. The details of these traps are compared to the ones in the current study in Table 5.

By comparison with the Arrhenius plots, it is clear that E_a is similar to a defect found in swift heavy ion irradiated GaN by Ngoepe *et al.* [33]. Although Ngoepe *et al.* [33] state that the defect they found agrees with the E2 found by Cho *et al.* [34], we found that the E2 in [34] is actually closer to E_b, as discussed below. This leaves identification of the E_a uncertain, but we speculate that it might be related to heavily damaged GaN, as would be the case after irradiation with swift heavy ions.

By comparing Arrhenius plots, the closest defect to E_b reported in literature was by Nguyen *et al.* [25] and Soh *et al.* [35] in GaN grown by metalorganic vapor phase epitaxy on sapphire and cracked GaN templates, respectively. It was also found in low concentrations by Arehart *et al.* [30] in molecular beam epitaxy grown GaN grown on sapphire with a GaN overlayer. From the broadness of the peak, Nguyen *et al.* [25] deduced that the peak is due to an extended defect.

Another nearby defect was observed by Hacke *et al.* [36] and Cho *et al.* [34], which, according to [34] is related to the nitrogen anti-site, however there is a significant difference in the Arrhenius plots of the two defects.

The spectrum of Sample *a* shows a shoulder to the right of the dominant peak at approximately the same position as E_b. We therefore conclude that E_b is present in both samples, albeit at different concentrations. The broad slowly decreasing shoulder to the left of Ea in Sample *a* may be due to the same defect in a high stress or high field environment (e.g. at grain boundaries) that causes emission rate enhancement. Alternatively, Ea and its shoulder might be due to a band of interfaces states at the grain boundaries as described by Broniatowski [37].

Sample *b* shows a similar broad shoulder which could be due to a lower concentration of E_a present in the sample. This is also hinted to by the slight asymmetry of E_b peak. We therefore conclude that both E_a and E_b are probably present in both samples, but in different concentrations. The reason for the growth rate favouring the one or the other is not clear. Further investigations in this regard are needed. Since the samples probably contain many other electrically inactive defects, or defects outside our measurement range, the DLTS measurements cannot be used to gauge the total defect concentration in the sample.

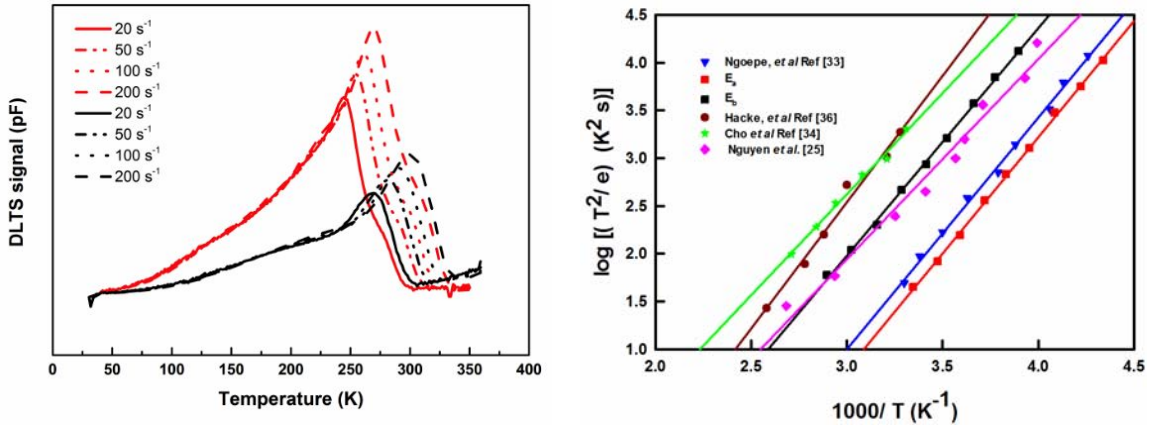

(a) (b)

Figure 7: (a) DLTS spectrum of Au/Ni/GaN Schottky diodes as-grown on Si under different conditions measured at a quiescent reverse bias of -2 V and filling pulse voltage of 0 V, rate window of 20 to 200 s^{-1} (the red plots represent Sample *a* and the black Sample *b*), and (b) the Arrhenius plots of deep-level defects present in the two samples compared to values found in literature.

Table 5: Defect parameters for the two GaN films grown on Si substrates by electrodeposition.

Current study			Similar defect		
Defect label	Activation energy (eV)	Capture cross section cm^2	Activation energy (eV)	Capture cross section cm^2	Label and Ref
E_a	0.49	8.6×10^{-15}	0.48	1.5×10^{-15}	$E_{0.48}$ [32]
			0.41	2.6×10^{-17}	E_{T2} [25]
			0.40	-	$E_{0.40}$ [30]
E_b	0.48	4.5×10^{-16}	0.60	1.61×10^{-15}	E2 [34]
			0.59	9×10^{-16}	A_5 [35]
			0.591	2.9×10^{-15}	ΔE2 [36]

Fig. 8 shows the depth profile of the defect concentration of Samples *a* and *b* obtained using different reverse bias voltages during the DLTS measurement. As can be seen from Fig. 8 the defect in Sample *b* had a concentration of roughly three times that in Sample *a*. In Sample *b*, there were more defects and a higher leakage current. This was consistent with the SEM image of Sample *b*, which showed a crack due to the higher growth rate and less relaxation.

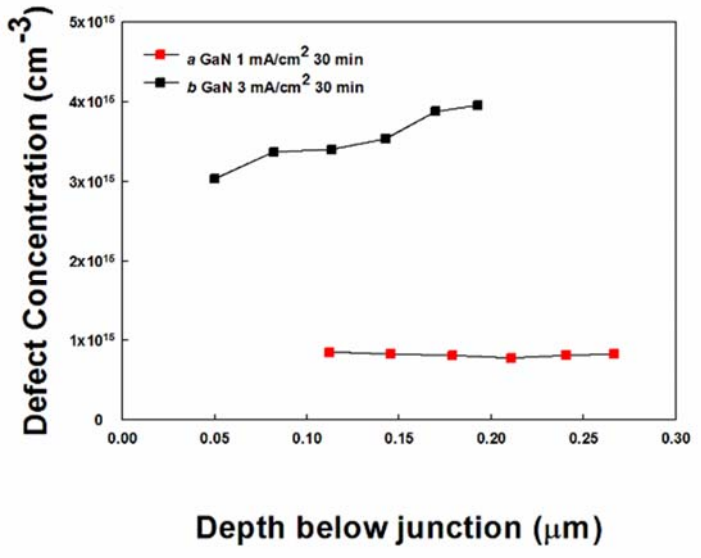

Figure 8: Depth profiles of defect concentration for the single defect found in Samples *a* and *b*.

4. Conclusion

Gallium nitride polycrystalline thin films were successfully prepared by electrodeposition. X-ray diffraction showed predominantly the hexagonal wurtzite structure. The shift in the diffraction angles (2 theta) could be attributed to changes in the current densities used for growth, which resulted in changes in the structural properties of thin films in Samples *a* and *b*.

The current transport in both samples were dominated by the thermionic emission with high series resistance. The electrical properties of Sample *a*, and Sample *b* were similar in terms of the general shape. Sample *a* showed much better rectifying properties than Sample *b*. The Schottky barrier height from *IV* and *CV* measurements for Samples *a*, and *b* were determined to be 0.76 eV and 0.60 eV from *IV*, while 0.92 and 0.71 eV from *CV*, respectively. Ideality factors were 1.8 and 2.3 with series resistances of 416 Ω and 241 Ω. *CV* carrier concentrations were between 1.2×10^{16} and 1.7×10^{16} cm^{-3}. In this study, Au/Ni Schottky diodes outperformed Au Schottky diodes on similar material in terms of ideality factor and barrier height. A model by Korsh & Muller [24] describing current flow through a polycrystalline medium fitted the data in the higher voltage region reasonably well, and a grain boundary potential of 0.29 V was extracted. Significant deviation of the fit in the low-voltage regions indicate that there is probably barrier height inhomogeneiety across the surface of the diodes.

DLTS measurements revealed two electron traps which were found to have activation energies of 0.49 and 0.48 eV, for Samples *a*, and *b*, respectively, although both samples show indications of both traps being present albeit at different concentrations. Broad shoulders to the lower temperature indicate the effect of electric field or stress enhancing the emission rates of the peaks, or might be a band of defects. Although a clear identification of the defects was not possible, it is likely that both are related to complex defects.

Acknowledgement

The authors would like to thank the South African National Research Foundation (NRF) for financial support during this study under Grant number 111744. The authors would also like to thank reviewer #3 for referring us to reference [22].

References

[1] Henini, M., & Razeghi, M. (2004). Optoelectronic Devices: III Nitrides. *Elsevier*.

[2] Morkoç, H. (2009). Handbook of nitride semiconductors and devices, Materials Properties, Physics and Growth. *John Wiley and Sons*.

[3] Puchinger, M., Wagner, T., Fini, P., Kisailus, D., Beck, U., Bill, J. & Lange, F. F. (2001). Chemical solution deposition derived buffer layers for MOCVD-grown GaN films. *Journal of Crystal growth*, *233*(1-2), 57-67.

[4] Kuykendall, T., Pauzauskie, P., Lee, S., Zhang, Y., Goldberger, J., & Yang, P. (2003). Metalorganic chemical vapor deposition route to GaN nanowires with triangular cross sections. *Nano Letters*, *3*(8), 1063-1066.

[5] Hsu, J. W. P., Manfra, M. J., Molnar, R. J., Heying, B., & Speck, J. S. (2002). Direct imaging of reverse-bias leakage through pure screw dislocations in GaN films grown by molecular beam epitaxy on GaN templates. *Applied Physics Letters*, *81*(1), 79-81.

[6] Jasinski, J., Swider, W., Liliental-Weber, Z., Visconti, P., Jones, K. M., Reshchikov, M. A. & Lee, K. Y. (2001). Characterization of free-standing hydride vapor phase epitaxy GaN. *Applied Physics Letters*, *78*(16), 2297-2299.

[7] Yadav, B. S., Major, S. S., & Srinivasa, R. S. (2007). Growth and structure of sputtered gallium nitride films. *Journal of Applied Physics*, *102*(7), 073516.

[8] Kim, O. H., Kim, D., & Anderson, T. (2009). Atomic layer deposition of GaN using Ga Cl 3 and NH 3. *Journal of Vacuum Science & Technology A: Vacuum, Surfaces, and Films, 27*(4), 923-928.

[9] Qiu, H., Cao, C., & Zhu, H. (2007). Synthesis of nanocrystalline GaN by the sol–gel method. *Materials Science and Engineering: B*, *136*(1), 33-36.

[10] Roy, R. K., and Pal, A. K. (2005). Synthesis of gallium nitride films by a novel electrodeposition route. *Materials Letters*, *59*(17), 2204-2209.

[11] Al-Heuseen, K., & Hashim, M. R. (2011). One-step synthesis of GaN thin films on Si substrate by a convenient electrochemical technique at low temperature for different durations. *Journal of Crystal Growth*, *324*(1), 274-277.

[12] Kang, J., Mitsuhashi, T., Kuroda, K., & Okido, M. (2019). Low-temperature synthesis of GaN film from aqueous solution by electrodeposition. *Journal of Applied Electrochemistry*, *49*(9), 871-881.

[13] Arias, A.C., Ready, S.E., Lujan, R., Wong, W.S., Paul, K.E., Salleo, A., Chabinyc, M.L., Apte, R., Street, R.A., Wu, Y. and Liu, P., (2004). All jet-printed polymer thin-film transistor active-matrix backplanes. *Applied Physics Letters*, *85*(15), pp.3304-3306.

[14] Zhan, Y., Mei, Y. and Zheng, L., (2014). Materials capability and device performance in flexible electronics for the Internet of Things. *Journal of Materials Chemistry C*, *2*(7), pp.1220-1232. doi. 10.1039/c3tc31765j.

[15] Ali, A. I., Danga, H. T., Nel, J. M., & Meyer, W. E. (2021). Deep-level transient spectroscopy of GaN grown by electrochemical deposition and irradiated with alpha particles. *Materials Science in Semiconductor Processing*, 127, 105685.

[16] Ngoepe, P. N. M., Meyer, W. E., Auret, F. D., Omotoso, E., & Diale, M. (2017). DLTS characterization of defects in GaN induced by electron beam exposure. *Materials Science in Semiconductor Processing*, *64*, 29-31.

[17] Calarco, R., Meijers, R. J., Debnath, R. K., Stoica, T., Sutter, E., & Lüth, H. (2007). Nucleation and growth of GaN nanowires on Si (111) performed by molecular beam epitaxy. *Nano letters*, *7*(8), 2248-2251.

[18] Auret, F. D., Meyer, W. E., Goodman, S. A., Koschnick, F. K., Spaeth, J. M., Beaumont, B., & Gibart, P. (1999). Metastable-like behaviour of a sputter deposition-induced electron trap in n-GaN. *Physica B: Condensed Matter*, *273*, 92-95.

[19] PŁaczek-Popko, E., Trzmiel, J., Zielony, E., Grzanka, S., Czernecki, R., & Suski, T. (2009). Deep level transient spectroscopy signatures of majority traps in GaN p–n diodes grown by metal-organic vapor-phase epitaxy technique on GaN substrates. *Physica B: Condensed Matter*, *404*(23-24), 4889-4891.

[20] Bahadormanesh, B., & Dolati, A. (2010). The kinetics of Ni–Co/SiC composite coatings electrodeposition. Journal of alloys and compounds, 504(2), 514-518.

[21] Patterson, A. L. (1939). The Scherrer formula for X-ray particle size determination. *Physical Review*, *56*(10), 978.

[22] Card, H. C., and Hwang, W. (1980). On the transport theory of Schottky barriers to polycrystalline silicon thin films. *IEEE Transactions on Electron Devices*, *27*(4), 700-705.

[23] Roll, G. (2012). Leakage current and defect characterization of short channel MOSFETs (Vol. 2). *Logos Verlag Berlin GmbH*.

[24] Korsh, G. J., & Muller, R. S. (1978). Conduction properties of lightly doped, polycrystalline silicon. *Solid-State Electronics*, *21*(8), 1045-1051.

[25] Nguyen, X. S., Hou, H. W., De Mierry, P., Vennéguès, P., Tendille, F., Arehart, A. R., Ringel, S. A., Fitzgerald, E. A., Chua, S. J. Chua, S. J. (2016). Deep level traps in semi-polar n-GaN grown on patterned sapphire substrate by metalorganic vapor phase epitaxy. *physica status solidi (b)*, *253*(11), 2225-2229.

[26] Arivazhagan, P., Ramesh, R., Kumar, R. R., Faulques, E., Bennis, F., & Baskar, K. (2016). Structural and electrical characteristics of GaN, n-GaN and $A1_xGa_{1-x}N$. *Journal of Alloys and Compounds*, *656*, 110-118.

[27] Thao, C. P., & Kuo, D. H. (2018). Electrical and structural characteristics of Ge-doped GaN thin films and its hetero-junction diode made all by RF reactive sputtering. *Materials Science in Semiconductor Processing*, 74, 336-341.

[28] Lee, S. Y., Jang, C. O., Hyung, J. H., Kim, T. H., & Lee, S. K. (2008). High-temperature characteristics of GaN nano-Schottky diodes. *Physica E: Low-dimensional Systems and Nanostructures*, *40(10)*, 3092-3096.

[29] Sanjay, S., & Baskar, K. (2018). Fabrication of Schottky barrier diodes on clump of gallium nitride nanowires grown by chemical vapour deposition. *Applied Surface Science*, *456*, 526-531.

[30] Arehart, A. R., Corrion, A., Poblenz, C., Speck, J. S., Mishra, U. K., & Ringel, S. A. (2008). Deep level optical and thermal spectroscopy of traps in n-GaN grown by ammonia molecular beam epitaxy. *Applied Physics Letters*, *93*(11), 112101.

[31] Pak, S. W., Lee, D. U., Kim, E. K., Park, S. H., Joo, K., & Yoon, E. (2013). Defect states of a-plane GaN grown on r-plane sapphire by controlled integration of silica nano-spheres. *Journal of crystal growth*, 370, 78-81.

[32] Lee, M., Vu, T. K. O., Lee, K. S., Kim, E. K., & Park, S. (2018). Electronic states of deep trap levels in a-plane GaN templates grown on r-plane sapphire by HVPE. *Scientific reports*, 8(1), 1-5.

[33] Ngoepe, P. N. M., Meyer, W. E., Auret, F. D., Omotoso, E., Hlatshwayo, T. T., Skuratov, V. A., & Diale, M. (2017). Deep level transient spectroscopy characterisation of Xe irradiated GaN. *Nuclear Instruments and Methods in Physics Research Section B: Beam Interactions with Materials and Atoms*, *409*, 69-71.

[34] Cho, H. K., Kim, C. S., & Hong, C. H. (2003). Electron capture behaviors of deep level traps in unintentionally doped and intentionally doped n-type GaN. *Journal of Applied Physics*, *94*(3), 1485-1489.

[35] Soh, C. B., Chua, S. J., Lim, H. F., Chi, D. Z., Liu, W., & Tripathy, S. (2004). Identification of deep levels in GaN associated with dislocations. *Journal of Physics: Condensed Matter*, *16*(34), 6305.

[36] Hacke, P., Detchprohm, T., Hiramatsu, K., Sawaki, N., Tadatomo, K., & Miyake, K. (1994). Analysis of deep levels in n-type GaN by transient capacitance methods. *Journal of Applied Physics*, *76*(1), 304-309.

[37] Broniatowski, A. (1987). Measurement of the grain-boundary states in semiconductors by deep-level transient spectroscopy. *Physical Review B*, *36*(11), 5895.